Neuron

Article

Distinct neural codes in primate hippocampus and lateral prefrontal cortex during associative learning in virtual environments

Highlights

- We trained monkeys to use a joystick to navigate in a VR learning task
- The hippocampus and lateral prefrontal cortex both encode information about the task
- Hippocampal neurons frequently fire in bursts with interspike intervals of <7 ms
- Information encoded in hippocampal burst rates is almost as high as that in firing rates

Authors

Benjamin W. Corrigan, Roberto A. Gulli, Guillaume Doucet, ..., Kartik S. Pradeepan, Adam J. Sachs, Julio C. Martinez-Trujillo

Correspondence

julio.martinez@robarts.ca

In brief

In this issue of Neuron, Corrigan et al. (2022) show that in monkeys carrying out a learning task in VR, neurons in the hippocampus and lateral prefrontal cortex use neural codes that are likely specialized for their respective long- and short-term memory functions.

Corrigan et al., 2022, Neuron *110*, 2155–2169
July 6, 2022
https://doi.org/10.1016/j.neuron.2022.04.016

CellPress

Neuron

CellPress

Article

Distinct neural codes in primate hippocampus and lateral prefrontal cortex during associative learning in virtual environments

Benjamin W. Corrigan,[1,2,3] Roberto A. Gulli,[4,5] Guillaume Doucet,[6] Megan Roussy,[1,2,3] Rogelio Luna,[1,2] Kartik S. Pradeepan,[1,2,3] Adam J. Sachs,[6] and Julio C. Martinez-Trujillo[1,2,3,7,8,*]

[1]Department of Physiology and Pharmacology, University of Western Ontario, London, ON, Canada
[2]Robarts Research Institute, University of Western Ontario, London, ON, Canada
[3]Brain and Mind Institute, University of Western Ontario, London, ON, Canada
[4]Zuckerman Mind Brain Behavior Institute, Columbia University, New York, NY, USA
[5]Center for Theoretical Neuroscience, Columbia University, New York, NY, USA
[6]The Ottawa Hospital, University of Ottawa, Ottawa, ON, Canada
[7]Lawson Health Research Institute, London, ON, Canada
[8]Lead contact
*Correspondence: julio.martinez@robarts.ca
https://doi.org/10.1016/j.neuron.2022.04.016

SUMMARY

The hippocampus (HPC) and the lateral prefrontal cortex (LPFC) are two cortical areas of the primate brain deemed essential to cognition. Here, we hypothesized that the codes mediating neuronal communication in the HPC and LPFC microcircuits have distinctively evolved to serve plasticity and memory function at different spatiotemporal scales. We used a virtual reality task in which animals selected one of the two targets in the arms of the maze, according to a learned context-color rule. Our results show that during associative learning, HPC principal cells concentrate spikes in bursts, enabling temporal summation and fast synaptic plasticity in small populations of neurons and ultimately facilitating rapid encoding of associative memories. On the other hand, layer II/III LPFC pyramidal cells fire spikes more sparsely distributed over time. The latter would facilitate broadcasting of signals loaded in short-term memory across neuronal populations without necessarily triggering fast synaptic plasticity.

INTRODUCTION

The primate lateral prefrontal cortex (LPFC) and hippocampus (HPC) are two brain regions that integrate high-level sensory information and play an important role in memory function. Lesion studies have shown that the HPC plays a fundamental role in long-term memory formation, for which HPC microcircuits possess enhanced synaptic plasticity (Bittner et al., 2017). On the other hand, the LPFC (areas 9/46) is known to play a fundamental role in short-term memory encoding, specifically layer II/III (Arnsten, 2013; Spaak et al., 2017). Short-term memories (e.g., briefly being able to remember a telephone number) are encoded in patterns of neural activity across populations of neurons that vanish after a few seconds (Leavitt et al., 2017). It is reasonable to assume that short-term memories do not necessarily trigger long-term synaptic plasticity. We hypothesize that the neural codes underlying neuronal communication and information processing in the primate HPC and layer II/III LPFC microcircuits are spatiotemporally tailored to service the corresponding memory functions of the two structures.

A mechanism that links trains of action potentials to synaptic plasticity is temporal summation: a compression of synaptic events over time that produces coincidence of postsynaptic potentials and triggers plastic changes in individual synapses (Kandel et al., 2012). Neuronal firing patterns that cluster spikes over short time intervals such as bursts can produce temporal summation and therefore induce synaptic plasticity (Thomas et al., 1998; Remy and Spruston, 2007). Burst firing in individual neurons is often found in brain areas associated with long-term memory formation, such as the HPC (Bliss and Collingridge, 1993; Lisman, 1997). However, burst firing has also been reported in the prefrontal cortex, classically associated with encoding short-term memories (Womelsdorf et al., 2014). An issue that has not been thoroughly studied in primates is how the ability to fire bursts of action potentials compares between HPC and LPFC neurons during behavior.

In the monkey prefrontal cortex, spike bursts in layer V neurons are associated with the onset of selective attention and are synchronized with the phase of beta and gamma frequencies in anterior cingulate cortex (Womelsdorf et al., 2014). However, during working memory (WM) tasks, most studies in the primate LPFC have computed spike rates over a second or more and documented the existence of persistent firing in layer II/III (Leavitt et al., 2017). Using linear classifiers, some studies have shown

that spike rates computed over at least 400- to 500-ms intervals maximize decoded information (Leavitt et al., 2017; Roussy et al., 2021), suggesting that LPFC neurons fire spikes sparsely over such intervals.

One possibility is that the time structure of the spike train in the HPC and the LPFC is "tailored" to perform different functions. In the HPC, spikes may be concentrated in bursts to maximize the probability of plastic changes in individual synapses via temporal summation. This would be in line with the primary role of the HPC in long-term memory formation (Eichenbaum et al., 2016). In the LPFC, spikes may be more sparsely distributed over time, which may favor information encoded over a larger population of neurons that can temporarily maintain and broadcast short-term memory signals locally and to other brain areas without necessarily triggering synaptic plasticity. The latter would be compatible with the role of neurons in LPFC layer II/III encoding short-term memory (Fuster and Alexander, 1971; Constantinidis and Goldman-Rakic, 2002).

Here, we compare the prevalence of spike train bursts and their relationship to task performance in the HPC and LPFC of macaque monkeys performing a spatial navigation associative memory task in a virtual environment. We found that neurons in both structures encode information about task variables (e.g., task periods and memory associations). However, HPC neurons more often compress spikes into bursts relative to LPFC layer II/III neurons. In the HPC, but not in the LPFC, bursts increase in frequency as performance improves as animals learn the task. We demonstrate that it is possible to decode task-related information from burst rates in the HPC with similar accuracy to decoders using spike rates. On the other hand, in the LPFC, burst-rate decoders performed substantially worse than spike-rate decoders. Additionally, we demonstrate that HPC neurons encode task-related information over shorter time windows and with fewer neurons relative to the LPFC.

RESULTS

We trained 4 monkeys (*Macaca mulatta*) on a context-object association task and recorded the responses of neurons from area CA3 of the HPC of two animals and from layer II/III of LPFC area 9/46 in the other two animals. During the task, animals navigated through a virtual X maze using a joystick (Figures 1A and 1B). Upon arriving at a decision point, where the maze branched out into two arms, two objects appeared at the arms' ends. The animal had to navigate toward one of the objects to obtain a reward. The target object was defined by the contingency of two features, the object's color and the walls' texture; e.g., for objects cyan and green: when the texture of the maze walls was wood, the target was cyan, whereas for a steel wall texture the target was green (see Figure 1D; STAR Methods; Gulli et al., 2020). Monkeys learned new associations every day until they became proficient at the task (see example in Figure 1C). Different color-wall texture associations were achieved by changing the target colors while leaving the wall (contexts) the same across sessions. In a 50-trial performance assessment window (see STAR Methods), they achieved average performances of 75.8% (monkey W, HPC), 61.3% (monkey R, HPC), 74.5% (monkey T, LPFC), and 84.3% (monkey B, LPFC) correct trials. The theoretical chance performance in this two-alternative forced-choice task was 50%. We also trained the LPFC monkeys on a WM task where they were cued to one of 9 locations in a virtual arena, and after a 3-s memory delay, they had to navigate to the cued position (Figures 1E and 1F; see Roussy et al., 2021).

Prevalence of burst firing in HPC and LPFC single neurons

We recorded the responses of neurons in the HPC using single electrodes (Figure 1G) and in the LPFC using microelectrode arrays (Utah arrays, 10 × 10 electrodes, 1.5-mm electrode length) implanted in area 9/46, ventral and dorsal to the principal sulcus targeting layer II/III (Figure 1H). Data were spike sorted and single action potential times were extracted and synchronized to task events. We classified neurons in each area into narrow and broad spiking (Figures S1A and S1B). This method shows some inaccuracies at separating putative interneurons from pyramidal cells (Torres-Gomez et al., 2020). However, considering that the majority of the neurons in the cortex are pyramidal cells (DeFelipe, 2012; DeFelipe et al., 2013; Yuste et al., 2020), we restricted our analyses to broad-spiking neurons and assumed that they were in their majority pyramidal cells. Pyramidal cells broadcast information between brain regions, and in structures such as the HPC and the LPFC, they play a fundamental role in memory coding. We recorded from putative pyramidal cells, 205 in the HPC over 37 sessions and 333 in the LPFC over 2 sessions (see STAR Methods). We quantified the firing rates of these neurons in both areas during the different task periods. Spikes of HPC neurons frequently occurred within 7 ms intervals (example in Figure 2A and blue spikes in Figure 2C). This was not the case for LPFC neurons, which fired more sparsely (example in Figures 2B and 2D). Indeed, when comparing the interspike interval (ISI) distributions of the two example units per trial period, the HPC unit shows a bias to short ISIs (Figure 2E) compared with the LPFC unit (Figure 2F).

We examined the probability density function for ISIs across all broad-spiking neurons during the period between the start and the end of the task, including the inter-trial intervals, in the two regions (Figures 3A and 3B). HPC neurons had a large peak below a bursting threshold of 7 ms ISIs compared with the LPFC. Additionally, we calculated the rate of change for ISI values, and in the HPC distribution it approaches 0 at around 7 ms (Figure 3A, inset) but remains close to 0 after a brief onset transient in LPFC. This suggests that HPC neurons frequently fire bursts with ISIs at around 7 ms. We further measured a burst fraction which quantifies the proportion of ISIs at or below 7 ms (Figures 3C and 3D). HPC neurons had a significantly higher burst fraction (median = 0.092) than LPFC neurons (median = 0.027) (rank-sum test, $Z(216,367) = 10.45$, $p < 0.05$) (Figure 3D). We noticed that as the firing rate increases, the probability of ISIs being below 7 ms increases in the LPFC (Pearson correlation coefficient $r = 0.67$, $p < 0.05$). This was not the case in the HPC, where the correlation was not statistically significant ($r = -0.06$, $p > 0.05$). The positive correlation between burst fraction and firing rate in LPFC neurons may suggest that their ISI distribution is approximated by a Poisson distribution (with some deviance as it approaches 0).

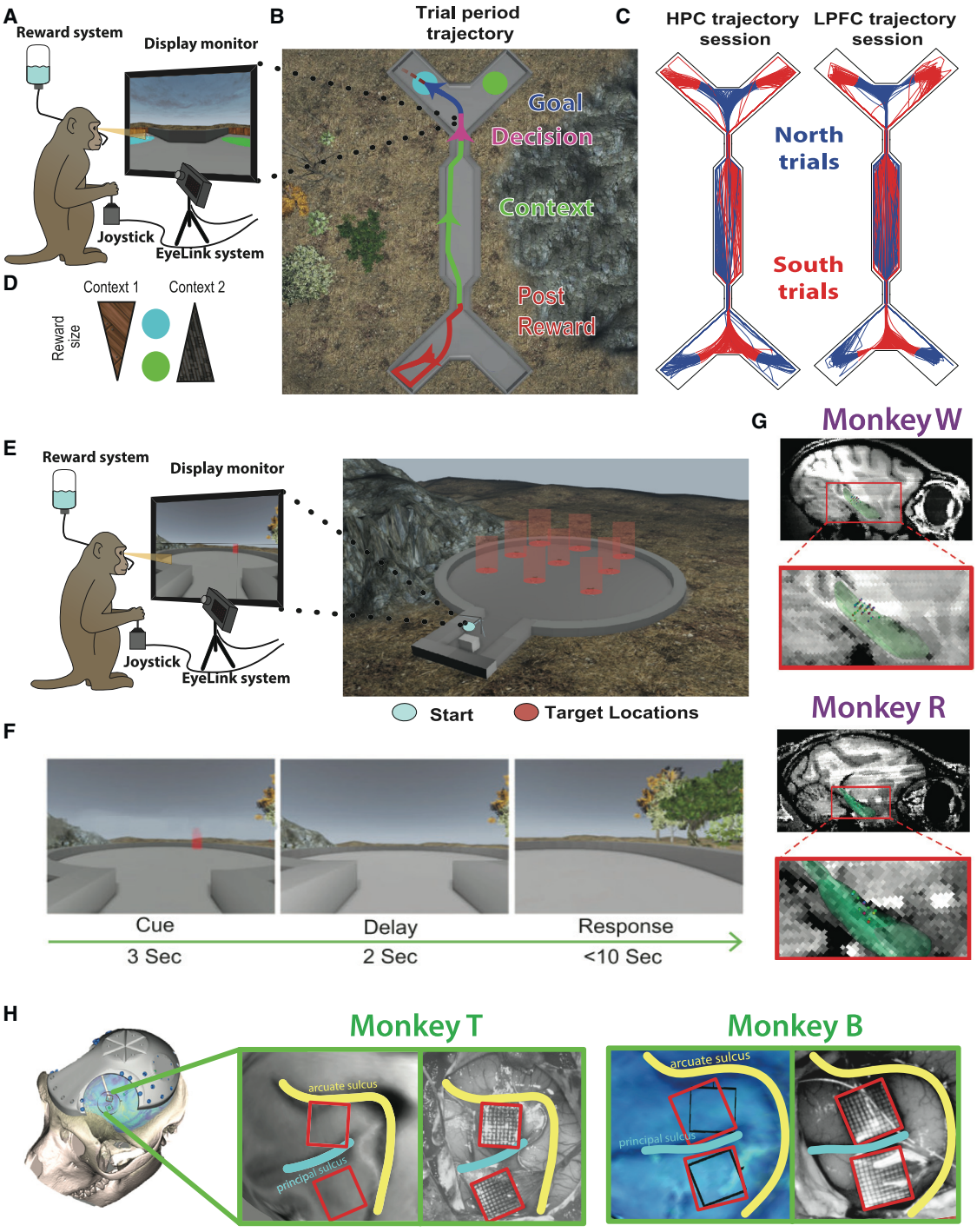

Figure 1. Recording from monkeys during virtual navigation learning task

(A) Experimental setup where monkeys were seated in front of a monitor and used a joystick to navigate the virtual environment. Eye position was monitored, and juice used as reward.

(B) Top-down view of maze with example trajectory split into four different task periods: post reward, context, decision, and goal (approach).

(C) Example sessions from monkeys and from each area showing all trajectories separated into north and south trials.

(D) The rule example defined cyan as the higher value object in context one (wood), and lower in context two (steel), and the inverse for the green object.

(E) Setup for virtual spatial working memory control task. Monkeys were again seated in front of a monitor and used a joystick to navigate. Image of arena has potential target locations indicated in red.

(F) Still images of the screen during an example trial.

(G) MRI-based reconstruction of recording positions in the right HPC of monkeys W and R.

(H) Array locations on area 9/46 for monkeys B and T.

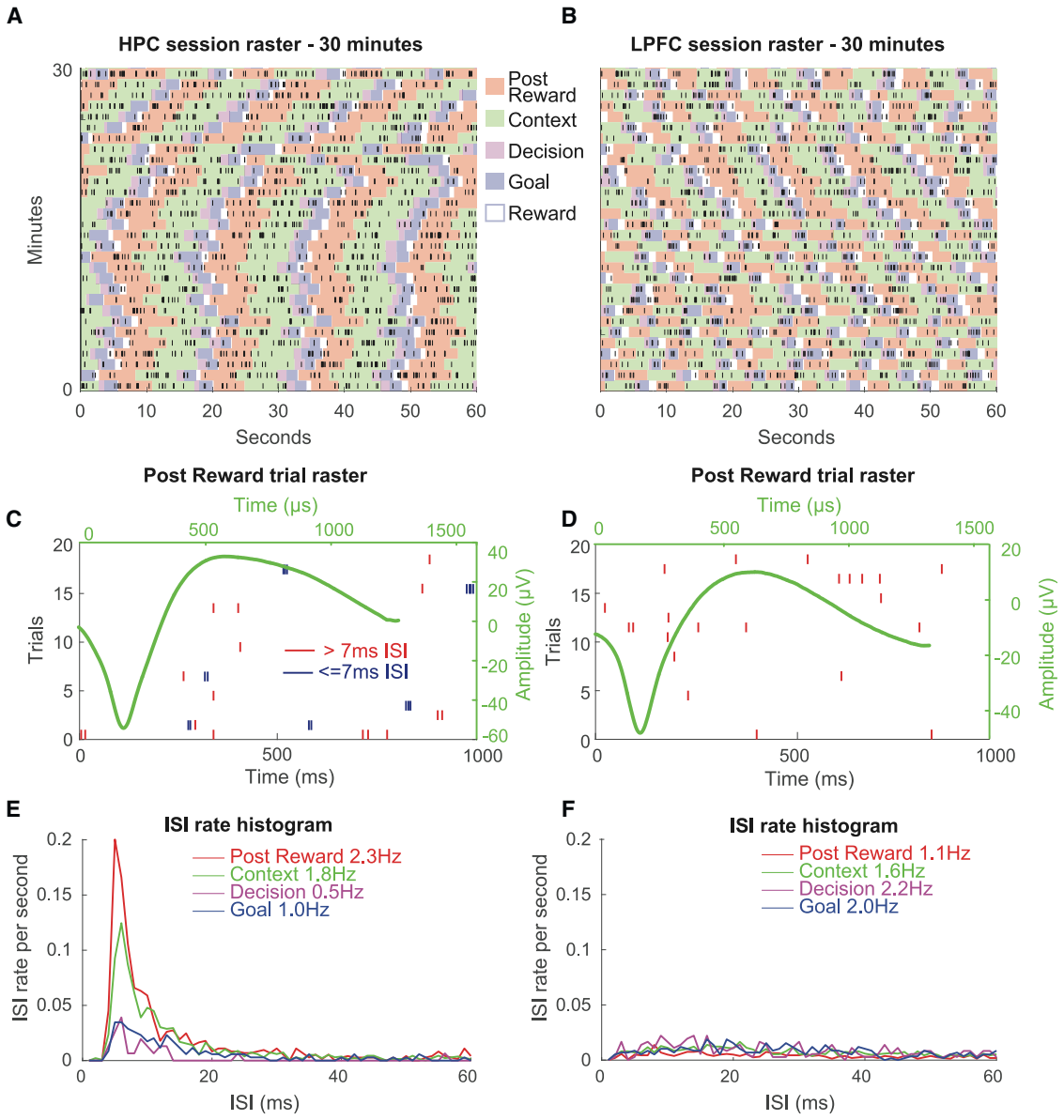

Figure 2. Differences in firing patterns between two example units in HPC and LPFC

(A and B) Session rasters showing example unit activity for 30 min, with background indicating the different trial periods.

(C and D) Trial rasters for the post-reward period with ISIs ≤7 indicated, occurring more frequently in the HPC. The example unit's waveform is superimposed, comprising broad-spiking neurons with a similar task firing rate of 1.8 Hz.

(E and F) ISI rate distributions for the different periods. Note that the HPC unit has much more activity below 20 ms than in the following 20 ms, whereas the LPFC unit has a more uniform distribution.

We used a method from Livingstone et al. (1996) to compute a probability distribution for ISIs as a function of firing rate relative to that predicted by Poisson firing neurons. For each neuron, we computed a burst index (BI, see STAR Methods), a bounded ratio of the measured ISIs, and the Poisson-predicted ISIs below a threshold of 7 ms. A positive value means shorter ISIs than predicted by a Poisson distribution and suggests that the cell often fire bursts, while a value at or below 0 indicates the opposite. The BI of HPC cells (median = 0.14) was significantly higher than the BI of LPFC cells (median = −0.11, $Z(216,367) = 8.60$, $p < 0.05$) (Figure 3E). The BI for LPFC cells did not correlate with firing rate ($r = -0.007$, $p > 0.05$). The BI for HPC cells was negatively correlated with the firing rate ($r = -0.42$, $p < 0.05$), indicating that as the firing rate increases, the BI decreases. This result seems counterintuitive. One likely explanation is that at low firing rates, many spikes in HPC neurons are concentrated within bursts, while at high firing rates, neurons fire spikes "outside" bursts. The latter leads to the same number of bursts, with increases in the number of spikes and consequently in the firing rate.

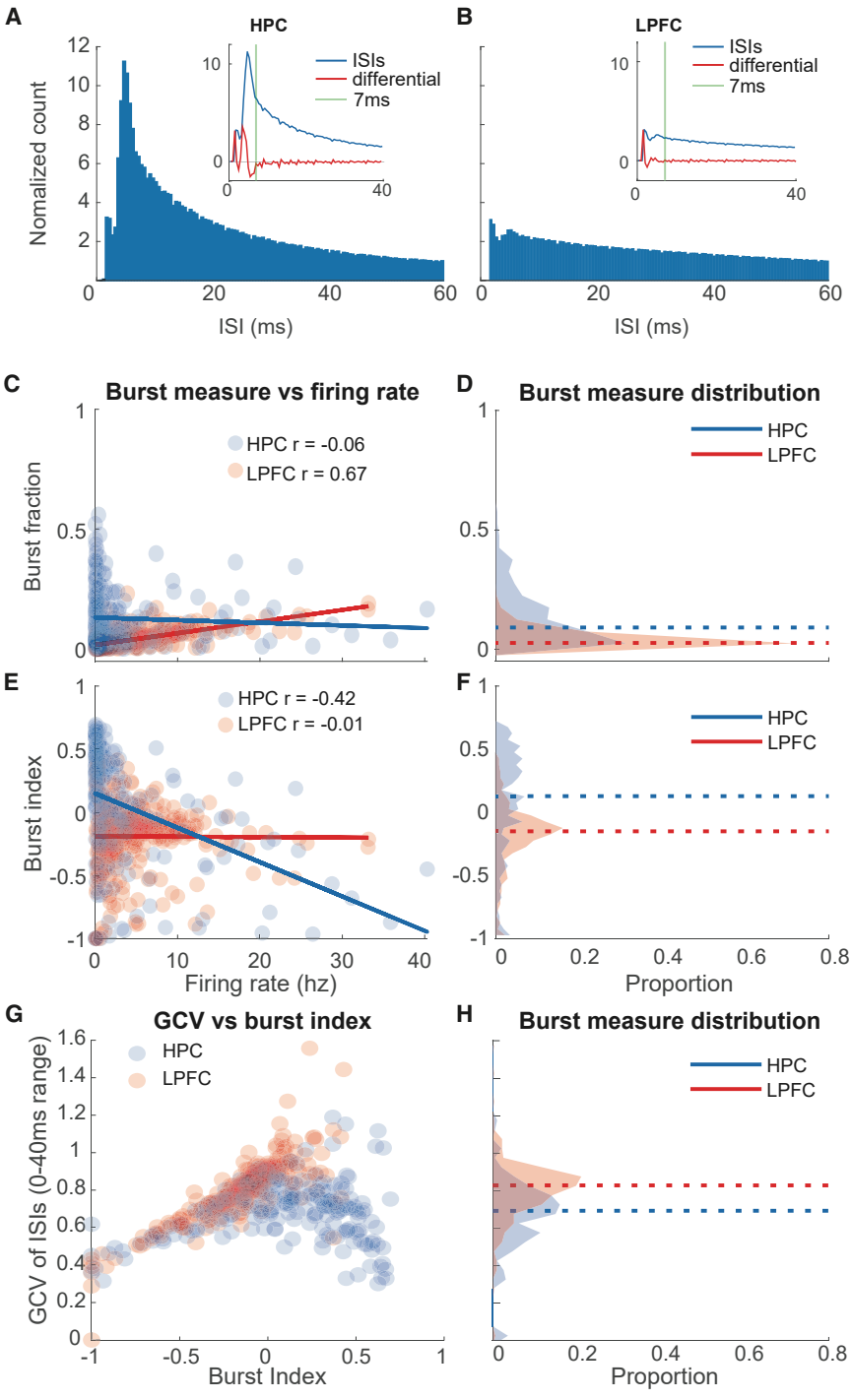

Figure 3. HPC cells are more prone to bursting, and the LPFC burst fraction is correlated with firing rate

(A) The probability density distribution of all ISIs for broad-spiking neurons in the HPC, normalized to the value at 60 ms. The HPC ISIs have a pronounced peak below the 7-ms burst threshold. The inset demonstrates the relationship between the distribution and its first derivative, which stabilizes after 7 ms.

(B) Same as (A), except for broad LPFC neurons.

(C) Burst fraction plotted against firing rate, where HPC cells have a high burst fraction at low firing rates.

(D) Population density of burst fractions.

(E) Same as (C), but with burst index (BI), where LPFC BI is no longer correlated with firing rate, and there is a slight negative correlation for the HPC.

(F) Population density of BI.

(G) GCV for ISIs between 0 and 40 ms plotted against BI. HPC GCV values decrease at high burst index values.

Distributions of BIs for different thresholds can be found in Figure S2. However, we carried out the rest of the analyses using the burst threshold of 7 ms because of the similar ranges found for other thresholds and the stabilization of the differential values at 7 ms (inset in Figure 3A). Some analyses may include other thresholds when required.

To rule out the possibility that increased HPC bursting was due to spike sorting issues that may have resulted in classifying multiple units as a single unit, we calculated a signal-to-noise ratio measure (d') (Leavitt et al., 2013; Figures S1C and S1D). We did not find a significant correlation between BI and d′ for HPC ($r = -0.01$, $p > 0.05$), and a small negative correlation for LPFC ($r = -0.037$, $p < 0.05$). These results suggest that any over estimation of burst occurrence may have happened in the LPFC; yet, bursts were more often found in HPC neurons, which argues against this variable acting as a confound to our main results. We also measured foveation durations to ensure that more frequent saccades were not generating more presaccadic bursts (Figure S7).

Finally, we calculated the geometric coefficient of variability (GCV, see STAR Methods; Equation 4) for ISIs between 0 and 40 ms. The GCV quantifies the variability of the ISIs. If spikes are generated within bursts with regular ISIs (see HPC example unit, Figure 2E), then the GCV will be low. If spikes are more sparsely distributed, with variable ISIs as in the LPFC example unit (Figure 2F), then the GCV will be high. We found that in both areas, GCV increases with BI for BI values below zero (Figure 3G). LPFC neurons continue this trend at BI > 0 (Figure 3G, red circles); however, HPC neurons with positive BI values do not: high BI HPC neurons show the lowest GCV values, indicating that bursts show highly regular ISIs and that they may be at least in part

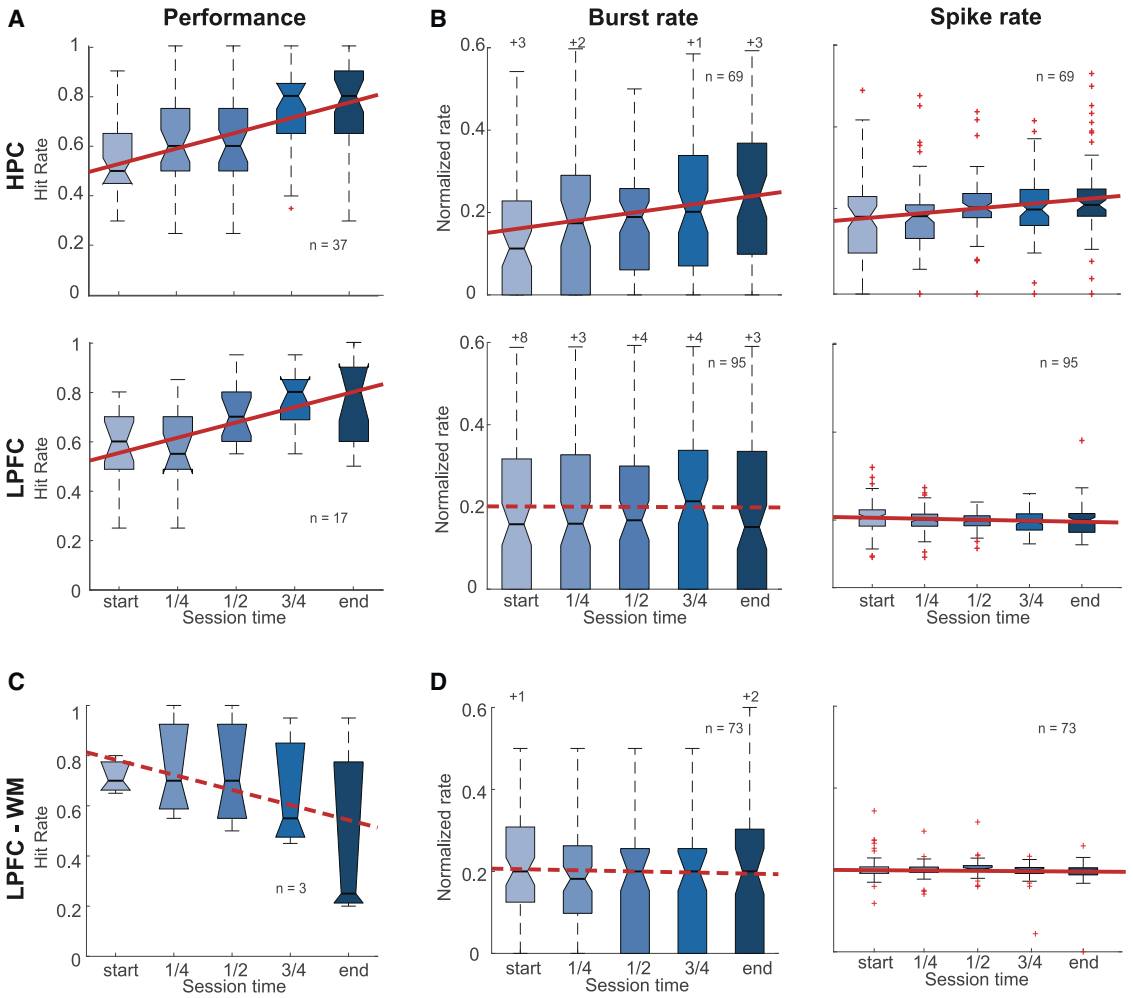

Figure 4. HPC bursting increases with performance, while LPFC bursting does not

(A) Performance defined by a hit rate for 20 trial blocks evenly spaced throughout each session for both the HPC and LPFC monkeys.

(B) Normalized burst and spike rates for blocks of 20 correct trials during the post-reward period. HPC bursts have a significant positive slope, as do HPC spikes, while LPFC bursts are stable and LPFC spikes have a slight significant negative slope. A comparison of burst rate and firing rate can be seen in Figure S3

(C and D) Same as (A and B), but for the working memory task in LPFC. Figure S3Boxes represent quartiles and error bars extend to the maximum value within 1.5 times the inter-quartile range, and numbers above distributions represent the number of outliers above the limit of the y-axis.

influenced by the intrinsic properties of these HPC neurons (blue circles in Figure 3G).

HPC bursting increases with task performance in post-reward period

We hypothesized that if bursting plays a role in learning and encoding of long-term memory, we should find a correlation between burst rates and task performance. To ascertain whether animals learned the association between the context and object color over the session, we binned the data in epochs of 20 trials, evenly distributed through the session (beginning, ¼, ½, ¾, and end) and calculated the mean performance rate for each epoch and for each session. There is a positive correlation between performance rate and time epoch for the 37 sessions with the HPC monkeys and the 17 sessions with the LPFC monkeys. The slope for the HPC sessions was 0.06 (95% CI = 0.04–0.08, Figure 4A), and the slope for the LPFC sessions was also 0.06 (95% CI = 0.04–0.08), indicating that animals learned the task at similar rates across all sessions. On the other hand, for the control WM task across 3 sessions, the slope was not significant (−0.06, 95% CI = −0.16–0.04, Figure 4C). These results suggest that improvement in performance across a session during the associative learning task was due to the animals learning the task.

We next measured the burst rate (number of bursts) and spike rate during five epochs of 20 correct trials evenly spaced throughout each session (Figure 4B). For HPC neurons that had bursts in at least two epochs, bursting increased (slope = 0.020, 95% CI = 0.007–0.033). The number of spikes also increased (slope = 0.012, 95% CI = 0.005–0.020). For the LPFC, bursting did not significantly increase (slope = −0.001, 95% CI = −0.013–0.012); however, the firing rate slightly

decreased (slope = −0.002, 95% CI = −0.004–−0.001). During the WM task, bursting in the LPFC did not change (slope = −0.003, 95% CI = −0.014–0.008, Figure 4D), and the spike rate slightly decreased (slope = −0.002, 95% CI = −0.004–−2e−5). The latter effect may be related to previous reports of decreases in spike rates in LPFC neurons when stimuli lose novelty (Wilson and Rolls, 1993; Miller and Desimone, 1994; Asaad et al., 1998). Changes during the associative learning task were not due to changes in burst rate over the time course of the session, since the results hold when correlating performance and burst rates independently of time during the session. We found a significant correlation between HPC bursts and hit rate ($r = 0.13$, $p < 0.05$), indicating that the previous result was not solely due to time during the session. On the other hand, HPC spike rates were not significantly correlated with performance ($r = 0.11$, $p > 0.05$). In the LPFC, both correlations were negative but not significant (LPFC bursts $r = -0.4$, $p > 0.05$, LPFC spikes $r = -0.07$, $p > 0.05$) (Figure S3). This result demonstrates that in the HPC, but not in the LPFC, bursting was positively correlated with improvements in performance as the animal learned the task.

Information about task periods encoded in burst and spike rates in HPC and LPFC

Beside the associative learning component, our task had different periods corresponding to different segments of the maze (post-reward, context, decision, goal approach, and reward). We examined whether neuronal spikes and/or bursts encoded information about the different task periods in the HPC and LPFC. For example, a neuron might respond to right turns during the goal approach period. An alternative might be a neuron that, during the post-reward period, integrates the reward feedback with the conjunction of the context and the chosen target in the previous trial. A deeper analysis of neuronal selectivities can be found in Gulli et al. (2020). Here, we will concentrate on task periods since our goal is to compare the information contained in burst and spike rates.

For each neuron, we computed mutual information during the first four task periods (post-reward, context, decision, and goal approach) for spike and burst rates, using a permutation test for significance. The spike rate was defined as the number of spikes that occurred during the entire task period divided by the period's duration. The burst rate was defined as the number of bursts (at least 3 spikes with ISIs <7 ms) during a task period, divided by the duration of the period. We also calculated burst rates with thresholds at 10, 15, and 20 ms (Figure S4), but most of our analyses focus on the 7-ms threshold. To ensure a reasonable sample size, we only used neurons with at least 60 completed trials. Additionally, we split cells based on BI values, with high bursting neurons (HBNs) having a $BI > 0$ and low bursting neurons (LBNs) having a $BI < 0$. The proportions of cells that were classified as HBN or LBN were different between areas. Of 192 HPC neurons, 131 (68%) were HBNs, whereas of 333 LPFC neurons, 69 (19%) were HBNs (rank-sum $z = 10.8$, $p < 0.05$).

From the 131 HBNs in the HPC, 71 (54%) encoded significant information about task periods; from those, 67 (94%) had significant spike-rate information and 43 (61%) had significant burst-rate information (Figure 5A). From the 69 HBNs in the LPFC, 52 (68%) encoded significant information about task periods; from those, 50 (96%) had significant spike-rate information, and 15 (29%) had significant burst-rate information (Figure 5A). The proportion of neurons with significant burst-rate information was significantly higher in the HPC (61%) than in the LPFC (29%, rank-sum $z = 3.48$, $p < 0.05$). From the 61 LBNs in the HPC, 70% encoded significant information about task periods; from those, 43 (100%) had spiking information and 5 (12%) had burst-rate information. These populations completely overlapped (Figure 5B). From the 264 LBNs in the LPFC, 200 (76%) encoded significant information about task periods; from those, 198 (99%) had spiking information and 25 (13%) had significant burst-rate information (Figure 5B). Unlike for HBNs, the proportions of neurons with significant burst-rate information for LBNs were similar (rank-sum $z = 0.16$, $p > 0.05$).

There were not only more cells with significant information in the spike rates, but the spike rates also had more information, on average, in the HBNs in both the HPC (burst median = 0.10, spike median = 0.14, rank-sum, $z = 2.48$, $p < 0.05$) and the LPFC (burst median = 0.08, spike median = 0.14, $z = 2.35$, $p < 0.05$) (Figure 5C). This was also the case for the LBNs in both the HPC (burst median = 0.10, spike median = 0.14, $z = 2.73$, $p < 0.05$) and the LPFC (burst median = 0.08, spike median = 0.15, $z = 2.23$, $p < 0.05$). When comparing information in HBNs, there was a significant difference between the HPC (median = 0.10) and the LPFC (median = 0.08), using a rank-sum test ($z = 2.04$, $p < 0.05$). In terms of the information available in the spikes, the HPC (median = 0.14) was not significantly different than the LPFC (median = 0.14, $z = 0.30$, $p > 0.05$). For the LBNs, there was no significant difference between the information available in the two areas in the bursts (HPC median = 0.10, LPFC median = 0.08, $z = 0.17$, $p > 0.05$) or in the spikes (HPC median = 0.14, LPFC median = 0.15, $z = 0.06$, $p > 0.05$). Thus, the HPC had a higher proportion of HBNs with significant information than the LPFC, and there was more information in the burst rates of HBNs in the HPC relative to the LPFC.

To further explore the effect that the burst threshold may have on mutual information, we calculated mutual information for thresholds at 10, 15, and 20 ms. Remarkably, for the HBNs in the HPC, the proportion of neurons with significant information was stable across the different thresholds (slope = 0.005, 95% CI = −0.007–0.018). In contrast, there were significant increases in the three other sub-populations: LPFC HBNs (slope = 0.010, 95% CI = 0.001–0.020), LPFC LBNs (slope = 0.020, 95% CI = 0.014–0.027), and HPC LBNs (slope = 0.038, 95% CI = 0.011–0.065, Figure 5D). One may consider that more neurons become significant as the threshold is increased, resulting in cells with significant spike-rate information, which have a more Poisson-like ISI distribution. The fact that the proportion of HBNs with significant information in the HPC is relatively stable across thresholds, suggests that bursting in these cells is tightly constrained and likely influenced by the neurons' intrinsic properties (Zeldenrust et al., 2018). These results show that for HBNs, burst rates in the HPC carry more information about task periods than in the LPFC. An analysis including a 4-ms bin is included in Figure S4.

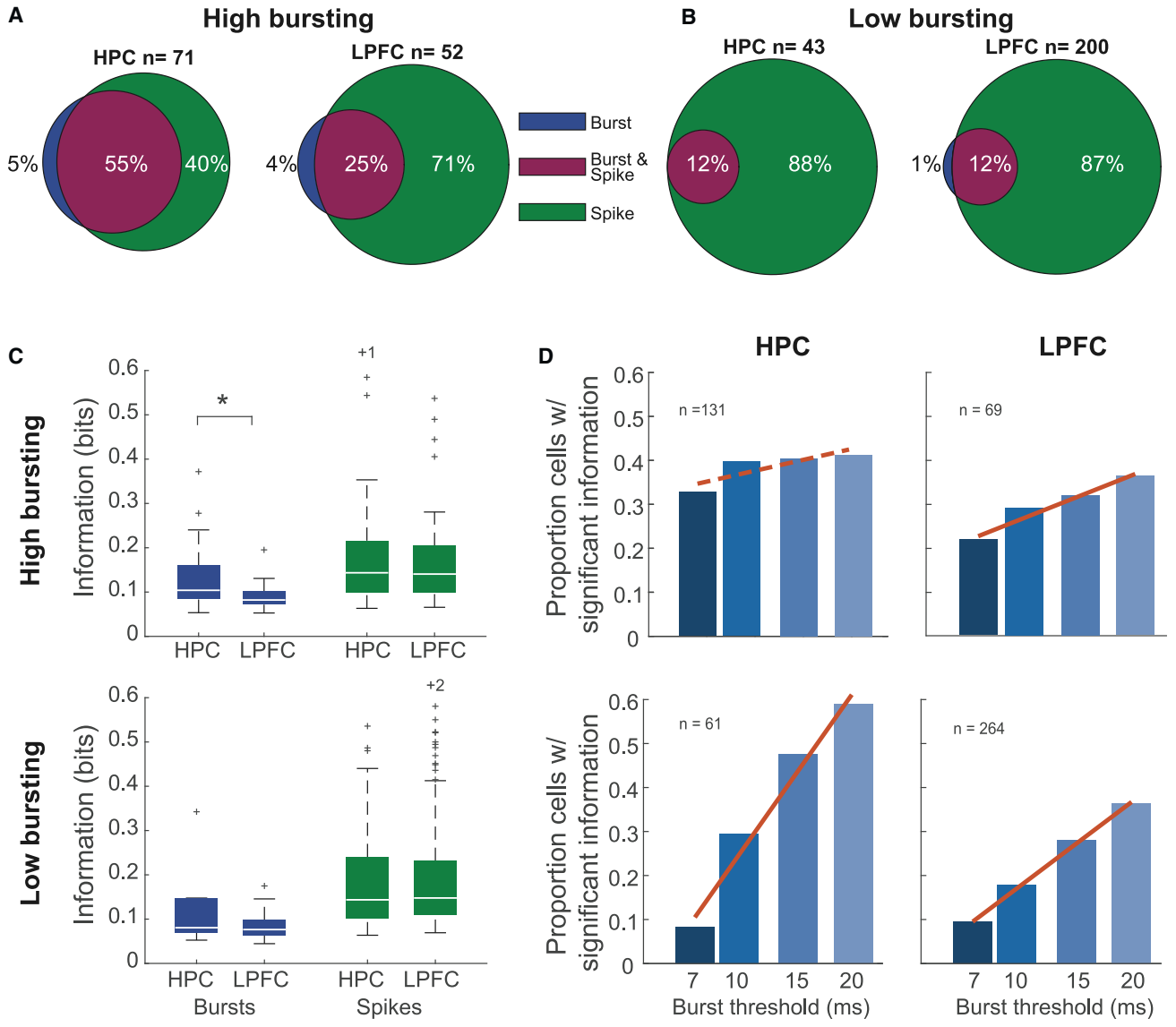

Figure 5. HPC high bursting neurons have more neurons with significant information, and these neurons have more bits of information than LPFC neurons

(A) Proportions of HBNs that have significant information in either the burst rate, the spike rate, or more often, both rates.

(B) Same as (A) but for LBNs.

(C) Amounts of information in bits for each significant neuron in HBN (above) and LBN (below) populations. Spikes have more information than bursts in all subpopulations. HPC HBNs have more information in the burst rate than LPFC neurons. Boxes represent quartiles and error bars extend to the maximum value within 1.5 times the inter-quartile range. * represent significant difference at $p < 0.05$.

(D) Proportion of cells that have significant information for different burst thresholds. Proportions significantly increase for every group except high bursting HPC. Fitted lines with significant slopes ($p < 0.05$) are represented as solid lines.

Decoding task-period information from bursts and spike rates in HPC and LPFC populations

To determine how results at the level of individual neurons generalize to populations, we conducted population-level analyses using linear classifiers. For the HPC, recordings were done over many days, so we constructed a pseudo-population of neurons by pooling neurons and drawing the same numbers of each trial period for each neuron (Mendoza-Halliday and Martinez-Trujillo, 2017). To compare LPFC data with HPC data, we shuffled the LPFC trial order, destroying simultaneity and the correlation structure of the population. Thus, the analyses use pseudo-populations of HBNs in both the HPC and the LPFC. We trained a support vector machine (SVM) to decode the trial period based on the spike rate or the burst rate from 60 trials of a subsampled pseudo-population of 60 cells from each area. We ran 5-fold cross-validation, getting one average performance, and then ran 50 subsamples to get 50 average performances. We also shuffled trial labels for each population to compute chance performances.

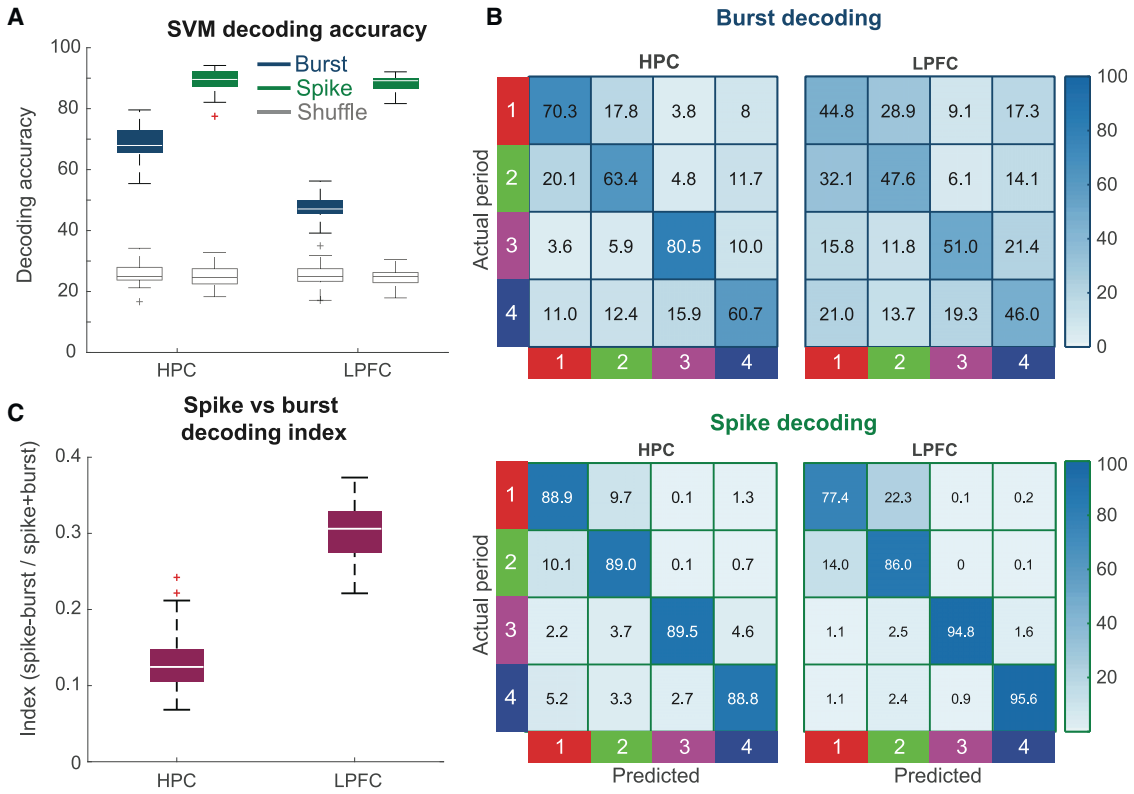

Figure 6. Population code for the HPC is similar between bursts and spikes, but not for the LPFC

(A) Average decoding accuracy for trial period in spike and burst codes in the two areas. All values are significantly different from the shuffles.

(B) Confusion matrices for burst and spike decoding in both areas. There is no distinct diagonal in LPFC burst decoding, but there is in the other three matrices.

(C) Spike-burst decoding index, where the difference between spike and burst decoding is significantly higher for the LPFC and close to 0 for the HPC. Decoding of task parameters in the goal approach period can be found in Figure S5. Boxes represent quartiles and error bars extend to the maximum value within 1.5 times the inter-quartile range.

All decoding performances were significantly different from chance performances, with no overlap between the confidence intervals for the actual values and the permutation values (Figure 6A). The HPC burst-rate decoding accuracy (median = 67.9%) was lower than the spike-rate decoding accuracy (median = 89.6%, permutation test, $p < 0.05$). In the LPFC, burst decoding accuracy (median = 47.1%) was lower than spike-rate decoding accuracy (median = 89.2%, $p < 0.05$). To contrast burst- versus spike-rate decoding between the two areas, we computed a spike-BI index (see STAR Methods Equation 5) (Figure 6C). There was a significant difference between the HPC index (median = 0.12, 32% higher performance for spike rates than burst rates) and the LPFC index (median = 0.31, 90% higher performance for spike rates than for burst rates) (t test, $t(98) = 23.8$, $p < 0.05$). Spike rates perform almost three times better than burst rates in the LPFC than in the HPC. Thus, although in the HBN spike rates were overall more informative than burst rates in both areas, burst rates had a more similar performance compared with spike rates in the HPC than in the LPFC.

One may argue that the lack of decoding in the LPFC from bursts may have been due to a lack of engagement in the associative learning task. This is unlikely since during the control WM task bursting was similar to that during the associative learning task (Figure S6A) and decoding of cued and memorized location from burst rates also performed significantly lower than from spike rates (Figures S6B). It could also be that the LPFC burst decoders performed worse than the burst decoders in the HPC because of differences in the number of periods without any activity (burst rates of 0 in the LPFC). To assess this, we calculated the percentage of periods in each session during which a neuron was silent, for both bursting and spiking activity (Figure S1E). Most neurons had a large percentage of periods without bursting activity, with the HPC having a similar median (97%) to the LPFC (98%) (rank-sum test, $z = 1.31$, $p > 0.05$). For spiking activity, the HPC had a significantly higher proportion of silent periods (median = 55%) compared with the LPFC (median = 7%, $z = 6.43$, $p < 0.05$). Importantly, for bursts there was not a significant difference in the proportion of "silent" periods between areas.

To explore how encoded information was distributed across neurons, we examined how decoded information from both burst and spike rates changes as a function of neuronal ensemble size and composition. We used the HBNs that had significant mutual information in their burst rates. We first estimated decoded information in individual neurons, and then we paired the most informative neurons with every other neuron to find the best duo, grouping that duo with every other neuron to

find the best trio, etc. (see Leavitt et al., 2017; Backen et al., 2018). We ran this process 50 times. For both the HPC and the LPFC, ensembles of a relatively small number of neurons saturated the decoder's performance (Figure 7A). We fit an exponential function to the data (Equation 6). All fits had an $r^2 > 0.95$. We calculated the point at 95% of the maximum performance to conduct comparisons between areas and burst- and spike-rate decoders. The HPC reached the 95% rate for spike rates at an average of 4.85 (SD = 1.30) neurons and for the burst rate at a similar number of 4.74 (SD = 1.25) neurons ($t(95) = 0.43$, $p > 0.05$). For the LPFC, firing rate ensembles reached the 95% point at an average of 4.50 (SD = 1.63) neurons and burst rate ensembles at a similar number of 4.20 (SD = 1.72) neurons ($t(97) = 0.90$, $p > 0.05$). The 95% point was not significantly lower for the LPFC than the HPC for firing rate decoders ($t(96) = 1.18$, $p > 0.05$), and there was no significant difference between the 95% points for the burst rates between areas ($t(96) = 1.79$, $p > 0.05$). Thus, ensembles with small numbers of neurons (~5) were sufficient to saturate the decoder's performance for both burst rates and spike rates.

To quantify the differences in performance between burst-rate decoders and spike rate decoders in each area, we computed a performance index. We used asymptotes of the performance equation for the 50 optimized decoders. For each decoder, we subtracted the burst-rate performance from the spike-rate performance and divided by the sum of the performances (Equation 5). The HPC performance index was lower (mean = 0.16, SD = 0.09) than the LPFC index (mean = 0.24, SD = 0.11; $t(98) = 4.40$, $p < 0.05$). These results indicate that burst rate contributes significantly more to information decoded in the HPC than in the LPFC and that in both areas task-period information can be decoded from small ensembles of neurons.

Effect of integration time windows in decoded information

To study the timescales over which both areas integrate information, we examined decoding performance as a function of integration time and window length for both areas. We used the same ensemble-building technique as in the previous analyses. However, instead of integrating over the entire task period, we took differently sized time windows centered at the middle of the period (i.e., 25, 50, 100, 150, 200, 300, 400, and 500 ms). We repeated the same curve fitting procedure as in Figure 7A and calculated the 95% point for all the curves (Figure 7B). Curves were normalized to the maximum asymptotic performance, which happened to be at the longest window (500 ms).

We found that the ensemble size at the 95% points was significantly lower for the HPC (mean = 7.0, SD = 0.45) than for the LPFC (mean = 8.3, SD = 0.56; paired t test, $t(7) = 8.82$, $p < 0.05$) (Figure 7B). We further calculated the performance of each ensemble as a fraction of the curve maximum for the average data in the 500-ms ensembles. The latter allows subtracting LPFC fractions from the HPC fractions for every time window and ensemble size to create an ensemble index (HPC-LPFC) that controls for differences in maximum performance between areas. A positive index means the HPC achieves a higher maximum decoding performance with the same ensemble size. A negative index means the opposite. A two-way ANOVA on the ensemble index was significant for both factors, time window size ($F(7) = 65.8$, $p < 0.05$) and ensemble size ($F(19) = 17.6$, $p < 0.05$); the interaction was not significant ($F(133) = 1.0$, $p > 0.05$). We further carried out two-sided t tests to determine which area—at an ensemble of size n and at a particular time point—performed better than the other. As demonstrated in Figure 7C, at lower ensemble sizes across all time windows, the HPC ensembles outperform the LPFC ensembles ($p < 0.05$). Remarkably, for the 25-ms time window, the HPC continues to outperform the LPFC for all ensemble sizes. These results demonstrate that HPC ensembles can "compress" more information into smaller time windows (25 ms) and using fewer units (up to 4) as compared with the LPFC.

DISCUSSION

Burst firing in HPC and LPFC neurons

Here we have used the definition of bursts as trains of action potentials that occur with close temporal proximity (<7 ms) or are more concentrated over time than predicted by a Poisson process. We found that the HPC has a larger proportion of putative principal neurons firing bursts than layer II/III of the LPFC. This agrees with previous studies in the HPC that have reported an abundance of burst firing in principal cells across species (Bliss and Collingridge, 1993; Lisman, 1997; Skaggs et al., 2007; Xu et al., 2012). It also agrees with studies in macaque LPFC layer II/III reporting that information decoded during WM and attention tasks is maximized when using time windows of 400 ms or longer (Backen et al., 2018; Leavitt et al., 2017; Tremblay et al., 2015). We should make clear that in both structures, spike rates (counting spikes inside and outside bursts) were more informative than burst rates. The latter suggests that not all informative spikes, even in the HPC, are compressed into bursts. Thus, the function of bursts may be diverse and not only related to information (Zeldenrust et al., 2018). Indeed, burst rates in the HPC, but not in the LPFC, increase with performance during the post-reward period of the associative memory task, suggesting that bursting may trigger fast synaptic changes in the HPC during learning (Harris et al., 2001). Such changes may occur to a lesser degree, slower, or more distributed in the LPFC.

Our results are unlikely due to differences in the type of information encoded by the HPC and LPFC neurons. Both the HPC (Doucet et al., 2020; Gulli et al., 2020) and the LPFC (Roussy et al., 2021) encode spatial information during virtual navigation. Additionally, both areas encode information about stimuli during associative learning tasks (Brincat and Miller, 2016; Gulli et al., 2020). Indeed, we show that neuronal populations in both areas encode task-period information; e.g., learning associations, spatial position in the virtual environment, or both (Figure S5). One may argue that the differences in the number of neurons firing bursts between the two areas is due to differences in the pattern of eye movements. Because saccades may be preceded by a burst, different numbers of saccades may lead to differences in bursting. In our task, animals could freely make saccades. Arguing against this explanation, we found that the durations of intersaccadic intervals, or foveations, are similar across HPC and LPFC animals (Figure S7). It is also unlikely that neurons

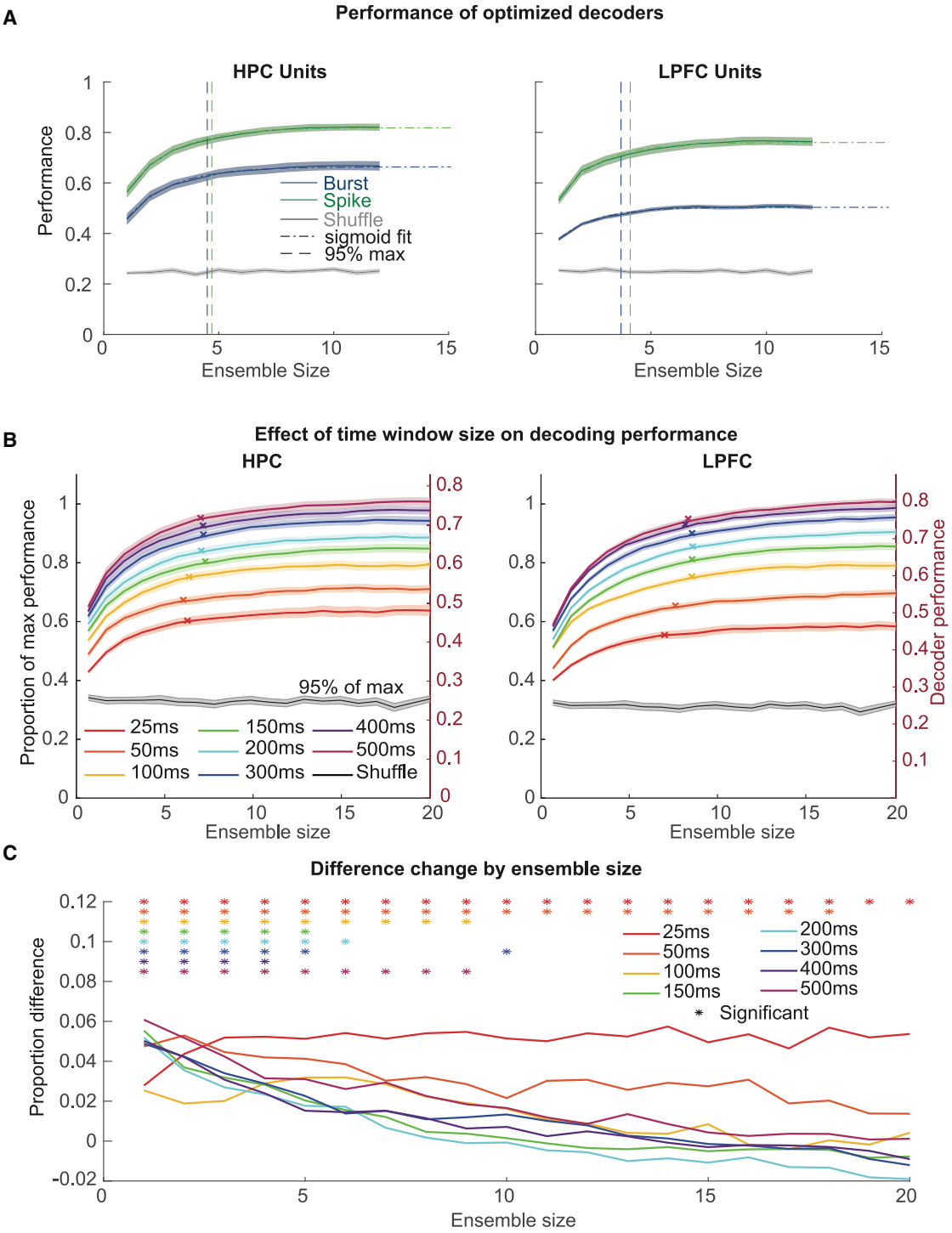

Figure 7. HPC firing rates carry information in compressed time windows and with fewer neurons

(A) Optimized ensembles for burst and spike rates yielded by neurons that have significant burst information, and their fits to Equation 6. HPC burst-rate ensembles are closer to the performance of HPC spike-rate ensembles in terms of maximum performance and position of the 95% threshold crossing. Shaded regions represent 95% confidence intervals.

(B) Optimized decoders for spike rate in different time windows, where HPC ensembles have a smaller range. Left axis is performance as a proportion of maximum achieved performance, and right axis is the raw performance. 95% of the maximum point is indicated with an "x" on each curve.

(C) HPC proportion of maximum performance minus LPFC proportion of maximum performance. The difference shows that for HPC, smaller ensembles perform better, as well as performing better in smaller time windows. Asterisks indicate significant difference from 0 ($p < 0.05$).

in the different areas encode saccade parameters linked to burst firing distinctively. A recent study has reported that during a naturalistic task only 2%–3% of LPFC neurons are tuned for saccade parameters (Roussy et al., 2021). In the HPC, neurons are generally not tuned for saccade parameters (Doucet et al., 2020; Gulli et al., 2020).

It has been reported that a feature of HPC principal cells is rapid burst firing, measured by ISIs below 20 ms (Lisman, 1997; Skaggs et al., 2007), or shorter, at 6–8 ms (Ranck, 1973; Buzsáki, 2015). Bursts can contain a significant proportion of all spikes, and a high burst fraction (fraction of all ISIs that are below 20 ms) is a distinguishing feature of HPC cells in primates (Skaggs et al., 2007) as well as rodents (Lisman, 1997). The HPC spike burst has consistently proven intriguing to scientists (Kepecs et al., 2002; Lisman, 1997; Zeldenrust et al., 2018). For example, bursts with short ISIs <6–8 ms are quite common along the perforant pathway, from the dentate gyrus to the subiculum regions (Mizuseki et al., 2012; Pernía-Andrade and Jonas, 2014; Simonnet and Brecht, 2019). It has been debated whether bursts can be the units of information coding in the HPC (Harris et al., 2001). Our results indicate that although there are also informative spikes outside the bursts, we could decode task-period information from burst rates with an accuracy close to that of spikes rates. This was not the case in the LPFC, where burst-rate decoding was close to chance and significantly lower than rate decoding. The latter suggests that LPFC spikes outside a burst play a larger role in information coding relative to the HPC.

In the macaque LPFC, few studies have examined the role of burst firing in the coding of WM signals (Constantinidis and Goldman-Rakic, 2002; Womelsdorf et al., 2014; Voloh and Womelsdorf, 2018). Constantinidis and Goldman-Rakic used an unbounded BI (comparing ISIs with predictions from a Poisson process) in LPFC neurons and found the median to be 0.9, just below 1, which would match the Poisson prediction. They calculated their index during the fixation period of an oculomotor delayed response task, where visual stimulation and dynamics were different from our virtual task. This may explain why they found 10% of cells with an index value $\geq$4, approximately 0.6 in our BI, but we found no LPFC neurons above 0.5. We also used a slightly larger window of ISIs, so this may have affected our results if ISI peaks drastically dropped off before 7 ms. Additionally, we were restricted to layer II/III of the LPFC, and their study may have included neurons in deeper layers that can be more prone to bursting (Womelsdorf et al., 2014). We did find bursting neurons in the LPFC. However, most of the informative spikes occurred outside the burst. Indeed, bursts rates in the LPFC performed poorly when used to decode information during the associative learning and WM tasks.

Memory functions of HPC and LPFC and relationship to bursts

A main hypothesis in our study was that neural codes in the HPC and LPFC have evolved to serve different memory functions. Bursting is more prevalent in the HPC and correlates with task performance when the trial information needs to be consolidated (Gulli et al., 2020). Given the relationship between burst firing, temporal summation, and synaptic plasticity, our results indicate that the prevalence of burst firing in the HPC serves long-term memory formation. Indeed, bursting has been shown to be more reliable than single spikes at producing postsynaptic potentials (Thomas et al., 1998; Remy and Spruston, 2007). A study (Xu et al., 2012) ablated excitatory postsynaptic potentials triggered by single spikes outside bursts by decreasing synaptotagmin-1 in rodent HPC CA1, but preserved the potentials triggered by burst spikes. Under these circumstances, learning was preserved. However, when they repeated the manipulation in the medial prefrontal cortex, learning was impaired. These results suggest that in the HPC, burst spikes play a fundamental role in memory formation, while spikes outside the burst play a lesser role. The inverse is true for the prefrontal cortex.

In the LPFC, spike rates integrated over long time intervals (>400 ms) provide the most information about items held in short-term memory (Leavitt et al., 2017; Roussy et al., 2021). Indeed, when we used the 2-s delay period, our decoders achieved high accuracy with spike rates, but when we used burst rates, accuracy dropped to chance (Figure S6C). This LPFC sparser code relative to the HPC may avoid triggering rapid synaptic plasticity and consolidation of all short-term memories, which would be counterproductive. Miller and colleagues have proposed that WM information can be stored in changes in synaptic weights that last hundreds of milliseconds (Miller et al., 2018). This is different from the plasticity that enables long-term memories to form and at the very least does not appear to be caused by bursts with ISIs below 7 ms across all neurons in the LPFC. Nevertheless, we did find bursting neurons in the LPFC during both tasks. These neurons may serve functions such as broadcasting and communication with other brain areas (Womelsdorf et al., 2014).

Two distinct architectures for two different memory functions

Differences in the neural codes employed by the HPC and LPFC may be due to different cortical architectures that serve different functions. The HPC contains three cortical layers (paleocortex) and relatively well-defined input and output pathways (O'Keefe and Nadel, 1978). The HPC cornu ammonis (CA) subfields have limited connectivity with the neocortex. Output from the HPC is almost exclusively through the subiculum and the entorhinal cortex. On the other hand, The LPFC is extensively connected to many other brain structures (Yeterian et al., 2012). The LPFC is organized in 6 cortical layers with a major expansion of layer II/III where neurons encoding WM have been identified (Constantinidis and Wang, 2004; Arnsten, 2013). Neurons in this region have extensive functional connectivity with one another that depends on their receptive and memory field location (Leavitt et al., 2013) and such fields cover the entire visual space (Bullock et al., 2017).

One interesting question would be whether *in vivo* burst-firing regimes in the HPC are mainly due to intrinsic properties of the principal cells or to network dynamics. Studies in rodents have shown that CA3 neurons also fire bursts *in vitro* when isolated from the rest of the brain (Ranck, 1973; Traub and Wong, 1981; Mizuseki et al., 2012). This bursting behavior may be required to induce processes such as long-term potentiation

(LTP) that enables coding of long-term memories (Bliss and Collingridge, 1993). Burst firing may be "built up" into the intrinsic machinery of the HPC principal cell rather than solely arising from the HPC networks' dynamics. Such intrinsic cellular machinery makes the HPC burst firing robust, enabling long-term memory formation under a variety of network firing regimes. However, one may also consider the role of network connectivity and dynamics adding heterogeneity and efficiency to neural communication and plasticity across the cortical mantle.

In the LPFC, a recent study has reported the existence of pyramidal cells in layer II/III that are intrinsically "bursty," based on their response profiles to square wave current pulses (González-Burgos et al., 2019). Interestingly, this study reported that burst neurons were more abundant in the LPFC relative to the lateral intraparietal area. Thus, it is possible that neocortical areas also differ in the way they cluster spikes over time, depending on their function and connectivity. The latter further indicates neural codes are heterogeneous and can serve different functions by changing their spatiotemporal features.

STAR★METHODS

Detailed methods are provided in the online version of this paper and include the following:

- KEY RESOURCES TABLE
- RESOURCE AVAILABILITY
  - Lead contact
  - Materials availability
  - Data and code availability
- EXPERIMENTAL MODEL AND SUBJECT DETAILS
- METHOD DETAILS
  - Electrophysiological recordings
  - Behavioral task
  - Behavioral analysis
  - Calculating spike width
  - Calculating burst propensity
  - Foveation analysis
  - Performance slope analysis
  - Burst and firing rate slopes
  - Calculating information
  - Decoding analysis
  - Optimized decoders
  - Working memory task analysis

SUPPLEMENTAL INFORMATION

Supplemental information can be found online at https://doi.org/10.1016/j.neuron.2022.04.016.

ACKNOWLEDGMENTS

We thank L. Duong for assistance in coding analyses. We thank B. Mahmoudian for input and discussion. We thank B. Bally, K. Barker, J. Blonde, S. Chisling, R. Kersten, W. Kucharski, S. Nuara, and K. Thomaes for technical assistance. This work was supported by the Natural Sciences and Engineering Research Council of Canada (NSERC) Postgraduate Scholarship-Doctoral Fellowship, Ontario Graduate Scholarship, Jonathan & Joshua Memorial Graduate Scholarship in Mental Health Research, and McGill David G. Guthrie Fellowship. This work was further supported by the Canadian Institutes of Health Research (CIHR), NSERC, BrainsCAN, and Neuronex (ref. FL6GV84CKN57) grants to J.C.M.-T.

AUTHOR CONTRIBUTIONS

B.W.C. collected and analyzed data and wrote the manuscript. R.A.G. designed the learning task and collected and analyzed data. G.D. contributed to the virtual environment design and data collection. M.R. designed the working memory task and collected and analyzed data. R.L. collected data. K.S.P. contributed to data analysis. A.J.S. contributed to surgical implantations. J.C.M.-T. contributed to experimental design and manuscript writing.

DECLARATION OF INTERESTS

The authors declare no competing interests.

Received: August 26, 2021
Revised: February 24, 2022
Accepted: April 14, 2022
Published: May 12, 2022

REFERENCES

Arnsten, A.F.T. (2013). The neurobiology of thought: the groundbreaking discoveries of Patricia Goldman-Rakic 1937–2003. Cereb. Cortex *23*, 2269–2281. https://doi.org/10.1093/CERCOR/BHT195.

Asaad, W.F., Rainer, G., and Miller, E.K. (1998). Neural activity in the primate prefrontal cortex during associative learning. Neuron *21*, 1399–1407. https://doi.org/10.1016/S0896-6273(00)80658-3.

Backen, T., Treue, S., and Martinez-Trujillo, J.C. (2018). Encoding of spatial attention by primate prefrontal cortex neuronal ensembles. eNeuro *5*. https://doi.org/10.1523/ENEURO.0372-16.2017.

Bittner, K.C., Milstein, A.D., Grienberger, C., Romani, S., and Magee, J.C. (2017). Behavioral time scale synaptic plasticity underlies CA1 place fields. Science *357*, 1033–1036. https://doi.org/10.1126/science.aan3846.

Bliss, T.V.P., and Collingridge, G.L. (1993). A synaptic model of memory: long-term potentiation in the hippocampus. Nature *361*, 31–39. https://doi.org/10.1038/361031a0.

Brincat, S.L., and Miller, E.K. (2016). Prefrontal cortex networks shift from external to internal modes during learning. J. Neurosci. *36*, 9739–9754. https://doi.org/10.1523/JNEUROSCI.0274-16.2016.

Bullock, K.R., Pieper, F., Sachs, A.J., and Martinez-Trujillo, J.C. (2017). Visual and presaccadic activity in area 8Ar of the macaque monkey lateral prefrontal cortex. J. Neurophysiol. *118*, 15–28. https://doi.org/10.1152/jn.00278.2016.

Buzsáki, G. (2015). Hippocampal sharp wave-ripple: A cognitive biomarker for episodic memory and planning. Hippocampus *25*, 1073–1188. https://doi.org/10.1002/hipo.22488.

Chang, C.-C., and Lin, C.-J. (2011). LIBSVM: A Library for Support Vector Machines. ACM Transactions on Intelligent Systems and Technology *2* (3), 1–27. https://doi.org/10.1145/1961189.1961199.

Constantinidis, C., and Goldman-Rakic, P.S. (2002). Correlated discharges among putative pyramidal neurons and interneurons in the primate prefrontal cortex. J. Neurophysiol. *88*, 3487–3497. https://doi.org/10.1152/jn.00188.2002.

Constantinidis, C., and Wang, X.-J. (2004). A neural circuit basis for spatial working memory. Neuroscientist *10*, 553–565. https://doi.org/10.1177/1073858404268742.

Corrigan, B.W., Gulli, R.A., Doucet, G., and Martinez-Trujillo, J.C. (2017). Characterizing eye movement behaviors and kinematics of non-human primates during virtual navigation tasks. J. Vis. *17*, 15. https://doi.org/10.1167/17.12.15.

DeFelipe, J. (2012). The neocortical column. Front. Neuroanat. *6*, 22. https://doi.org/10.3389/fnana.2012.00022.

Defelipe, J., López-Cruz, P.L., Benavides-Piccione, R., Bielza, C., Larrañaga, P., Anderson, S., Burkhalter, A., Cauli, B., Fairén, A., Feldmeyer, D., et al. (2013). New insights into the classification and nomenclature of cortical GABAergic interneurons. Nat. Rev. Neurosci. *14*, 202–216. https://doi.org/10.1038/nrn3444.

Doucet, G., Gulli, R.A., Corrigan, B.W., Duong, L.R., and Martinez-Trujillo, J.C. (2020). Modulation of local field potentials and neuronal activity in primate hippocampus during saccades. Hippocampus *30*, 192–209. https://doi.org/10.1002/hipo.23140.

Doucet, G., Gulli, R.A., and Martinez-Trujillo, J.C. (2016). Cross-species 3D virtual reality toolbox for visual and cognitive experiments. J. Neurosci. Methods *266*, 84–93. https://doi.org/10.1016/j.jneumeth.2016.03.009.

Eichenbaum, H., Amaral, D.G., Buffalo, E.A., Buzsáki, G., Cohen, N., Davachi, L., Frank, L., Heckers, S., Morris, R.G., Moser, E.I., et al. (2016). Hippocampus at 25. Hippocampus *26*, 1238–1249. https://doi.org/10.1002/hipo.22616.

Fuster, J.M., and Alexander, G.E. (1971). Neuron activity related to short-term memory. Science *173*, 652–654. https://doi.org/10.1126/science.173.3997.652.

González-Burgos, G., Miyamae, T., Krimer, Y., Gulchina, Y., Pafundo, D.E., Krimer, O., Bazmi, H., Arion, D., Enwright, J.F., Fish, K.N., et al. (2019). Distinct properties of Layer 3 pyramidal neurons from prefrontal and parietal areas of the monkey neocortex. J. Neurosci. *39*, 7277–7290. https://doi.org/10.1523/JNEUROSCI.1210-19.2019.

Gulli, R.A., Duong, L.R., Corrigan, B.W., Doucet, G., Williams, S., Fusi, S., and Martinez-Trujillo, J.C. (2020). Context-dependent representations of objects and space in the primate hippocampus during virtual navigation. Nat. Neurosci. *23*, 103–112. https://doi.org/10.1038/s41593-019-0548-3.

Harris, K.D., Hirase, H., Leinekugel, X., Henze, D.A., and Buzsáki, G. (2001). Temporal interaction between single spikes and complex spike bursts in hippocampal pyramidal cells. Neuron *32*, 141–149. https://doi.org/10.1016/S0896-6273(01)00447-0.

Kandel, E.R., Schwartz, J.H., and Jessell, T. (2012). Principles of neural science, Fifth Edition (McGraw-Hill).

Kepecs, A., Wang, X.-J., and Lisman, J. (2002). Bursting neurons signal input slope. J. Neurosci. *22*, 9053–9062. https://doi.org/10.1523/JNEUROSCI.22-20-09053.2002.

Leavitt, M.L., Pieper, F., Sachs, A., Joober, R., and Martinez-Trujillo, J.C. (2013). Structure of spike count correlations reveals functional interactions between neurons in dorsolateral prefrontal cortex area 8a of behaving primates. PLoS One *8*, e61503. https://doi.org/10.1371/journal.pone.0061503.

Leavitt, M.L., Pieper, F., Sachs, A.J., and Martinez-Trujillo, J.C. (2017). Correlated variability modifies working memory fidelity in primate prefrontal neuronal ensembles. Proc. Natl. Acad. Sci. USA *114*, E2494–E2503. https://doi.org/10.1073/pnas.1619949114.

Lisman, J. (1997). Bursts as a unit of neural information: making unreliable synapses reliable. Elsevier Curr. Trends *20*, 38–43. https://doi.org/10.1016/S0166-2236(96)10070-9.

Livingstone, M.S., Freeman, D.C., and Hubel, D.H. (1996). Visual responses in V1 of freely viewing monkeys. Cold Spring Harbor Symp. Quant. Biol. *61*, 27–37. http://www.ncbi.nlm.nih.gov/pubmed/9246432.

Mendoza-Halliday, D., and Martinez-Trujillo, J.C. (2017). Neuronal population coding of perceived and memorized visual features in the lateral prefrontal cortex. Nat. Commun. *8*, 15471. https://doi.org/10.1038/ncomms15471.

Miller, E.K., and Desimone, R. (1994). Parallel neuronal mechanisms for short-term memory. Science *263*, 520–522. https://doi.org/10.1126/science.8290960.

Miller, E.K., Lundqvist, M., and Bastos, A.M. (2018). Working memory 2.0. Neuron *100*, 463–475. https://doi.org/10.1016/J.NEURON.2018.09.023.

Mizuseki, K., Royer, S., Diba, K., and Buzsáki, G. (2012). Activity dynamics and behavioral correlates of CA3 and CA1 hippocampal pyramidal neurons. Hippocampus *22*, 1659–1680. https://doi.org/10.1002/hipo.22002.

O'Keefe, J., and Nadel, L. (1978). The Hippocampus as a Cognitive Map (Oxford University Press).

Pernía-Andrade, A.J., and Jonas, P. (2014). Theta-gamma-modulated synaptic currents in hippocampal granule cells *in vivo* define a mechanism for network oscillations. Neuron *81*, 140–152. https://doi.org/10.1016/j.neuron.2013.09.046.

Ranck, J.B. (1973). Studies on single neurons in dorsal hippocampal formation and septum in unrestrained rats. Part I. Exp. Neurol. *41*, 462–531. https://doi.org/10.1016/0014-4886(73)90290-2.

Remy, S., and Spruston, N. (2007). Dendritic spikes induce single-burst long-term potentiation. Proc. Natl. Acad. Sci. USA *104*, 17192–17197. https://doi.org/10.1073/pnas.0707919104.

Roussy, M., Luna, R., Duong, L., Corrigan, B., Gulli, R.A., Nogueira, R., Moreno-Bote, R., Sachs, A.J., Palaniyappan, L., and Martinez-Trujillo, J.C. (2021). Ketamine disrupts naturalistic coding of working memory in primate lateral prefrontal cortex networks. Mol. Psychiatry *26*, 6688–6703. https://doi.org/10.1038/s41380-021-01082-5.

Simonnet, J., and Brecht, M. (2019). Burst firing and spatial coding in subicular principal cells. J. Neurosci. *39*, 3651–3662. https://doi.org/10.1523/JNEUROSCI.1656-18.2019.

Skaggs, W.E., McNaughton, B.L., Permenter, M., Archibeque, M., Vogt, J., Amaral, D.G., and Barnes, C.A. (2007). EEG sharp waves and sparse ensemble unit activity in the macaque hippocampus. J. Neurophysiol. *98*, 898–910. https://doi.org/10.1152/jn.00401.2007.

Spaak, E., Watanabe, K., Funahashi, S., and Stokes, M.G. (2017). Stable and dynamic coding for working memory in primate prefrontal cortex. J. Neurosci. *37*, 6503–6516. https://doi.org/10.1523/JNEUROSCI.3364-16.2017.

Thomas, M.J., Watabe, A.M., Moody, T.D., Makhinson, M., and O'Dell, T.J. (1998). Postsynaptic complex spike bursting enables the induction of LTP by theta frequency synaptic stimulation. J. Neurosci. *18*, 7118–7126. https://doi.org/10.1523/jneurosci.18-18-07118.1998.

Timme, N.M., and Lapish, C. (2018). A tutorial for information theory in neuroscience. eNeuro *5*. https://doi.org/10.1523/ENEURO.0052-18.2018.

Torres-Gomez, S., Blonde, J.D., Mendoza-Halliday, D., Kuebler, E., Everest, M., Wang, X.J., Inoue, W., Poulter, M.O., and Martinez-Trujillo, J. (2020). Changes in the proportion of inhibitory interneuron types from sensory to executive areas of the primate neocortex: implications for the origins of working memory representations. Cereb. Cortex *30*, 4544–4562. https://doi.org/10.1093/CERCOR/BHAA056.

Traub, R.D., and Wong, R.K.S. (1981). Penicillin-induced epileptiform activity in the hippocampal slice: a model of synchronization of CA3 pyramidal cell bursting. Neuroscience *6*, 223–230. https://doi.org/10.1016/0306-4522(81)90058-0.

Tremblay, S., Pieper, F., Sachs, A., and Martinez-Trujillo, J. (2015). Attentional filtering of visual information by neuronal ensembles in the primate lateral prefrontal cortex. Neuron *85*, 202–215. https://doi.org/10.1016/j.neuron.2014.11.021.

Voloh, B., and Womelsdorf, T. (2018). Cell-type specific burst firing interacts with theta and beta activity in prefrontal cortex during attention states. Cereb. Cortex *28*, 4348–4364. https://doi.org/10.1093/cercor/bhx287.

Wilson, F.A.W., and Rolls, E.T. (1993). The effects of stimulus novelty and familiarity on neuronal activity in the amygdala of monkeys performing recognition memory tasks. Exp. Brain Res. *93*, 367–382. https://doi.org/10.1007/BF00229353.

Womelsdorf, T., Ardid, S., Everling, S., and Valiante, T.A. (2014). Burst firing synchronizes prefrontal and anterior cingulate cortex during attentional control. Curr. Biol. *24*, 2613–2621. https://doi.org/10.1016/j.cub.2014.09.046.

Xu, W., Morishita, W., Buckmaster, P.S., Pang, Z.P., Malenka, R.C., and Südhof, T.C. (2012). Distinct neuronal coding schemes in memory revealed

by selective erasure of fast synchronous synaptic transmission. Neuron *73*, 990–1001. https://doi.org/10.1016/j.neuron.2011.12.036.

Yeterian, E.H., Pandya, D.N., Tomaiuolo, F., and Petrides, M. (2012). The cortical connectivity of the prefrontal cortex in the monkey brain. Cortex *48*, 58–81. https://doi.org/10.1016/J.CORTEX.2011.03.004.

Yuste, R., Hawrylycz, M., Aalling, N., Aguilar-Valles, A., Arendt, D., Armañanzas, R., Ascoli, G.A., Bielza, C., Bokharaie, V., Bergmann, T.B., et al. (2020). A community-based transcriptomics classification and nomenclature of neocortical cell types. Nat. Neurosci. *23*, 1456–1468. https://doi.org/10.1038/s41593-020-0685-8.

Zeldenrust, F., Wadman, W.J., and Englitz, B. (2018). Neural coding with bursts—current state and future perspectives. Front. Comput. Neurosci. *12*, 48. https://doi.org/10.3389/fncom.2018.00048.

STAR★METHODS

KEY RESOURCES TABLE

REAGENT or RESOURCE	SOURCE	IDENTIFIER
Experimental models: Organisms/strains		
Rhesus macaques	Unspecified vendor	McGill University and Western University
Software and algorithms		
Matlab 2020a	MathWorks	https://mathworks.com/products/matlab.html RRID: SCR_001622
Libsvm 3.23	Chang and Lin, 2011	https://www.csie.ntu.edu.tw/~cjlin/libsvm/
Neuroscience Information Theory Toolbox	Timme and Lapish, 2018	https://doi.org/10.1523/ENEURO.0052-18.2018
Offline Sorter	Plexon	https://plexon.com/products/offline-sorter/
Other		
Utah arrays	Blackrock Microsystems	https://blackrockneurotech.com/research/utah-array/
Custom code	This paper	https://doi.org/10.5281/zenodo.6450233

RESOURCE AVAILABILITY

Lead contact

Further information and requests for resources should be directed to and will be fulfilled by the lead contact, Prof. Julio Martinez-Trujillo (julio.martinez@robarts.ca).

Materials availability

This study did not generate new unique reagents.

Data and code availability

All data reported in this paper will be shared by the lead contact upon request.

All original code has been deposited at zenodo.org and is publicly available as of the date of publication. DOIs are listed in the key resources table.

Any additional information required to reanalyze the data reported in this paper is available from the lead contact upon request.

EXPERIMENTAL MODEL AND SUBJECT DETAILS

Four male rhesus macaques (*Macaca mulatta*) were used in these experiments, two in HPC experiments (7 and 14 years old, and 7kg and 12kg respectively) and two in LPFC experiments (10 and 9 years old, 12kg and 10kg respectively). All procedures followed Canadian Council on Animal Care guidelines and were carried out at either McGill University or Western University and were approved by the respective University Animal Care Committees.

METHOD DETAILS

Electrophysiological recordings

HPC recordings were carried out using 1-4 high impedance (400-1500 kOhms) tungsten electrodes lowered each day to the right HPC, using co-registered image guidance for trajectory and depth, with examples seen in Figure 1G of recording locations. Most recordings were done in the mid to posterior putative CA3 region. Further information on electrode placement and targeting is available in Gulli et al. (2020). LPFC recordings were acquired using two 96-channel Utah arrays positioned at the posterior end of the principal sulcus, on the dorsal and ventral gyri of the principal sulcus and the anterior gyrus of the arcuate sulcus, targeting area 9/46. The shank length was 1.5mm, and was impacted into the brain, so was likely in layer II/III, and electrodes had an impedance ranging from 20 to 1500 kOhms. Signals were acquired at 30 kHz using one (HPC) or two (LPFC) 128-channel Cerebus recording systems (Blackrock Microsystems) and saved for later offline sorting, done with Plexon Offline sorter (version 4.5.0, Plexon Inc.). Spike sorting for the learning task was carried out by two experimenters (RAG and BWC) and sorting on all channels in both HPC

and LPFC was verified by BWC. Time was not used as a feature during sorting, but units with waveform shapes that varied extensively or merged with other units were excluded from these analyses. Spike sorting for the working memory task was semi-automated using the T-Distribution method in Offline Sorter before being manually refined by MR.

Behavioral task

The learning tasks were very similar, taking place in a double ended Y maze, termed the Xmaze and described previously (Doucet et al., 2016; Gulli et al., 2020). At the end of each Y, were two colored discs towards one of which the animals would navigate to receive the associated reward. The reward was dictated by the context, which was indicated by a texture that was applied to the walls, either a dark grey "steel" texture or a brown "wood" one. The highest value color in one context was the lowest in the other context (Figure 1D). The LPFC recordings were done with only this high and low option, but the HPC had a middle color that was worth half the reward in both contexts. Monkeys used the joystick to navigate to their chosen color, receive the associated reward, and then turn around and navigate back towards the other end to make another choice. Figure 1 shows an example trial trajectory, and the trajectories for two example sessions (Figures 1B and 1C).

The working memory task set-up was the same, however took place in a circular arena with a 3x3 array of potential target locations, and a starting area on the side from where the monkey started each trial (Figure 1E). Trials started with a Cue period where one of the 9 locations had a red fog presented for 3 seconds, followed by a 2 second Delay period, after which there was a 10 second Response period where the monkey had to navigate to the cued location. More information on task performance is included in Roussy et al. (2021).

Behavioral analysis

Monkeys were trained to be able to learn the task before recordings, and then presented with new combinations of colors each day, picked pseudo randomly to avoid a color occurring two days in a row. We used a performance analysis window of the 50 trials preceding the final 10 trials (excluded because performance may falter as satiation is reached).

Calculating spike width

To separate neurons into putative principal cells and interneurons, we started by interpolating the waveform signals to 1MHz, and then aligning the waveforms for a neuron to the minimum of the trough. We then calculated the mean waveform and measured the duration between the minimum (trough) and the maximum (peak) in microseconds (Figure S1A). To determine where to divide the neurons into narrow and broad spiking, for each area we fit two Gaussians, and used the local minimum as the threshold to separate them (HPC = 334μs, LPFC = 333μs). Because the results were within 1μs, we used the threshold for the LPFC as there were more neurons and it might be slightly more accurate. We then discarded all narrow neurons (<10%) because we did not have enough to analyze separately and focused our results on the putative pyramidal cells for the rest of the study.

Calculating burst propensity

The initial analysis of ISIs was just done by taking all spikes recorded from broad spiking neurons during the task and pooling them for each area. We removed all ISIs greater than 60ms and then normalized histograms to value at the stable period at 60ms for each area. To assess the stability of the curve of the population, we calculated the difference between each point and plotted it for the HPC. We calculated the burst fraction as the fraction of all ISIs during the task that were equal to or below 7ms. Because this could start to correlate with high firing rates, we also made a burst index (BI) for the neurons based on the ISI histogram and the predicted ISI distribution based on a Poisson distribution with the calculated firing rate. To predict the probability of ISIs of a certain duration, we followed the method of Livingstone et al. (1996), taking the firing rate averaged over the whole task. Using Equation 1, where λ = firing rate, and t = time bin. We calculated the probability for each 1ms time bin from 2-40ms, and then normalized these

$$f(t) = \lambda e^{-\lambda t} \quad \text{(Equation 1)}$$

measures by the sum of all these predictions. We then did the same thing with the measured ISIs, normalizing by the sum of the measured ISIs between 2 and 40ms. We then summed the predicted values from 2 to 7ms and subtracted that from the sum of the measured values between 2 and 7ms. We divided this difference by the sum of the two sums to bind our index between -1 and 1 (see Equation 2). We then repeated this for threshold values of 4, 10, 15 and 20ms.

$$burst\ index = \frac{\sum ISIs\ measured - \sum ISIs\ predicted}{\sum ISIs\ measured + \sum ISIs\ predicted} \quad \text{(Equation 2)}$$

To calculate the *d'* noise measurement, we measured the mean and the variance at three locations, the trough (minimum peak), the peak (maximum peak), and the first point at the baseline of the spike, before any spike deflections, to get a measure of the noise. We then calculated two *d'* values, one comparing the trough to the baseline, and the other comparing the peak to the baseline both using Equation 3. We then summed these two values and calculated the correlation with the BI (calculated at 7ms threshold).

$$d' = \frac{mean(peak) - mean(baseline)}{\sqrt{var(peak) - var(baseline}} \quad \text{(Equation 3)}$$

To calculate the geometric coefficient of variation (GCV) we analyzed only ISIs below 40ms, using Equation 4 where s is the standard deviation of ISIs. We used the GCV instead of the CV because the distribution of ISIs was not normal and was more similar to log-normal.

$$GCV = \sqrt{e^{s^2_{ln}} - 1} \quad \text{(Equation 4)}$$

Foveation analysis

It has previously been reported that saccades can be preceded by a pre-saccadic burst in neurons, and it is possible that this could be driving a difference between burst measures in the two areas if there were differences in eye-movement behavior between the monkeys. To assess this, we used the method from Corrigan et al., (2017) to classify eye position data into saccades and foveations, code for which can be found at https://github.com/JMTNeuroLab/VR_EyeSignalClassification. Briefly, saccades were identified based on acceleration thresholds, and then the onset and offset of saccades were defined based on deviation from main direction of the saccade, which would indicate that the movement of the saccade was no longer driving the signal, and direction changes were now driven by noise in the foveation. Periods between saccades were classified as foveations. We measured the durations of foveations as a proxy for frequency of saccades and compared the distributions across all sessions between the LPFC and HPC monkeys.

Performance slope analysis

To assess performance, we chose 5 epochs: the first 20 trials, the last 20 trials, and the 20 trials centered on the ¼, ½, and ¾ marks of the session. We simply calculated the hit rate for the sessions during these epochs, and then performed a regression to determine if there was a positive slope, indicating that hit rate increased over the course of the session. We included 15 other sessions (monkey T = 8, monkey B = 7) for the performance to show that the performance was consistent but did not analyze any neural data from these sessions. For the WM task, we analyzed three sessions (monkey T = 2, monkey B = 1) for both the behaviour and the neural data.

Burst and firing rate slopes

Similar to the performance analysis but restricted to periods after correct trials to control for reward effects. To calculate the rates of bursts or spikes, and to be able to use only correct trials that approximated the trials used to assess performance, we used 20 correct trials: the first 20, the last 20, and the 20 centered on the ¼, ½, and ¾ marks of the session. We only analyzed broad spiking neurons that had at least one burst in at least two epochs, analysing the same neurons for both the burst and spike rates. To normalize the values, we summed the rates across epochs, and used this value to divide each epoch's rate. We again ran a regression to determine if there was a consistent trend in the rates of bursts or spikes.

Calculating information

To calculate mutual information, we used only correct trials. Bursts were detected as any group of three or more spikes where all ISIs were equal or less than 7ms. The timing of the burst was the onset of the first spike, and which ever period the first spike occurred in was considered the period that the burst happened in. We split the task into four behaviorally separate periods: the post reward period, the context period, the decision period, and goal approach period. The post reward period started at the end of the reward administration and is potentially when the monkey is incorporating the knowledge gained from the previous trial. This continues until they navigate to the start of the corridor where the context appears, which is the start of the context period. The decision period starts at the appearance of the target objects, when they must choose between the two, and the goal approach period starts at the beginning of the first turn of more than 10 degrees towards an object, and proceeds until they reach the target, just before reward administration. The period of reward administration was not analyzed. The durations of each task period vary based on which period it is, and by trial, but we calculated rates based on the duration of each individual period. We only analyzed broad spiking neurons, and separated neurons into high bursting neurons (BI>0, HBNs) and low-bursting neurons (BI<0, LBNs) and analyzed these subpopulations separately. We used 60 sample rates from each trial period for each neuron to calculate the mutual information using the Neuroscience Information Theory Toolbox (Timme and Lapish, 2018). We then ran 5000 shuffles to generate the p-value for the mutual information via permutation. We then ran this whole process, starting from the subsampling, 50 times and analyzed the means of the mutual information and the p-value for each neuron.

We also repeated this whole analysis with burst thresholds set at 10ms,15ms and 20ms, and fit a line to the 4 proportions of units that had significant burst rate information to determine whether this proportion increased with the threshold for the different subpopulations.

Decoding analysis

For the decoding analysis, we used support vector machine (SVM) decoding from LIBSVM v.3.23 (Chang and Lin, 2011) using five-fold cross-validation and a linear kernel on rates that were normalized between 0 and 1. We only used broad spiking, HBNs and again randomly sampled 60 rate pairs from each trial period and ran the decoding analysis on each set of rates before shuffling the labels and decoding again to get a measure of chance decoding. We repeated this 50 times to take the mean accuracy and mean chance decoding of the same trials for both spike rate and burst rate decoding. Significance was determined by permutation test, where the

mean had to be greater than 95% of the shuffled performances to be significant. To examine the differences between the performance of the burst and spike decoder within an area, and to compare this across areas, we created a decoding index (see Equation 5). This gave us 50 index values to run a t test on.

$$\text{Spike} - \text{burst index} = \frac{\text{decoding accuracy for spike rate} - \text{decoding accuracy for burst rate}}{\text{decoding accuracy for spike rate} + \text{decoding accuracy for burst rate}} \quad \text{(Equation 5)}$$

To analyze navigation and task parameter signals, we used the decision period of correct trials, and separated them into left and right decisions, and based on the two colors chosen. This gave us 4 combinations, and we used a subsample of 30 trials from 30 neurons, and we again used 5-fold cross validation. We ran this process 50 times on different subsamples and reported the distributions of mean decoding accuracies achieved for both areas for bursts and spikes.

Optimized decoders

For the optimized ensembles, we used the same set up for the SVM, but for the pool of neurons we only used HBNs that had significant mutual information ($p < .05$) for a specific rate. This limited the number of neurons we could use. To control for differences in number of eligible neurons in the two areas, for an iteration of the optimized decoder, we would randomly select up to 30 neurons from which we would build the decoder. For the first test, we used only neurons with significant mutual information for burst rate, which limited us to only 15 cells in LPFC, so we used this population size for both areas. Each neuron was tested individually to find the neuron with the best decoding accuracy. This neuron was then paired with every other neuron, and we ran an SVM on each duo to find the best duo. The best duo was used to find the best trio that included the best duo, and so on. This does not necessarily find the absolute optimal duo or trio, but it is an effective method for exploring the decoding space without having to exhaustively try all possible permutations, which can be computationally expensive. Indeed, it results in better decoding accuracies than simply using the best neurons based on individual performance, as illustrated in Leavitt et al. (2017). After building the decoder to either 12 units for the initial analysis, or 20 units for the time window analysis (described below) we then selected another set of random units and repeated the process to build another optimized decoder, building 50 optimized decoders in total to give us a population of results to analyze.

For the decoders built to assess the contribution of neurons we only used neurons with significant information in the burst rate. We fit an exponential function (Equation 6) to each performance curve, and calculated the point where performance was 95% of the asymptote which is defined as 1-c. This gave us 50 points for each set of decoders so we could run t tests on these points within areas and within spike and burst rates, however, we discarded any ensembles that did not reach the 95% point within 3 standard deviations of the distribution of 95% points.

$$y = 1 - a * e^{-\left(\frac{x}{b}\right)} - c \quad \text{(Equation 6)}$$

The time window analysis used different time windows within which to calculate the rates. Because we wanted to analyze the compression of the full signal, we only used the firing rates for this analysis, and used neurons that had significant firing rate mutual information values. We used time windows of 25, 50, 100, 150, 200, 300, 400, and 500 milliseconds instead of integrating over the whole trial period. We chose to center the windows in the middle of the period. We built the optimized decoders with pools of 30 neurons, but only built them to 20 neurons because they would have already saturated decoding performance before then. We built 50 optimized decoders for each time window for each area. To fairly compare the effect of time windows, we took the maximum of the average performance across ensemble sizes of the best decoder (500ms) and calculated the performance of all the decoders, at each ensemble size, as a fraction of such maximum performance. To compare these performance fractions, we took the HPC fractions for each time window and sample size and subtracted the corresponding LPFC fractions, which gave us a population of differences at each ensemble size and time window. We ran a two-way ANOVA on these differences to assess for effects of time window size or ensemble size on the differences in performance. To determine which differences between the two areas were significantly different from 0, we calculated a one-sample *t*-test for each ensemble size and time window.

Working memory task analysis

We analyzed 2 sessions from monkey T and one form Monkey B and combined the neurons from each to analyze burst indices and decoding performance. We were unable to record any hippocampal data in this task. We calculated the burst index as indicated above, and then ran a Kolmogorov-Smirnov test to determine whether there was a difference between the BI for the learning task and the working memory task. We also ran a decoder on bursting and firing rates during the Cue and Delay periods to determine if there was encoding of the target column location (grouped into three columns, left, right and center). Again, running 50 subsamples of 19 trials in each category (57 total trials for each subsample).